JOURNAL OF GEOPHYSICAL RESEARCH, VOL. 116, C10036, doi:10.1029/2011JC007035, 2011

Complex mean circulation over the inner shelf south of Martha's Vineyard revealed by observations and a high-resolution model

Neil K. Ganju,[1] Steven J. Lentz,[2] Anthony R. Kirincich,[2] and J. Thomas Farrar[2]

Received 3 February 2011; revised 2 August 2011; accepted 10 August 2011; published 29 October 2011.

[1] Inner-shelf circulation is governed by the interaction between tides, baroclinic forcing, winds, waves, and frictional losses; the mean circulation ultimately governs exchange between the coast and ocean. In some cases, oscillatory tidal currents interact with bathymetric features to generate a tidally rectified flow. Recent observational and modeling efforts in an overlapping domain centered on the Martha's Vineyard Coastal Observatory (MVCO) provided an opportunity to investigate the spatial and temporal complexity of circulation on the inner shelf. ADCP and surface radar observations revealed a mean circulation pattern that was highly variable in the alongshore and cross-shore directions. Nested modeling incrementally improved representation of the mean circulation as grid resolution increased and indicated tidal rectification as the generation mechanism of a counter-clockwise gyre near the MVCO. The loss of model skill with decreasing resolution is attributed to insufficient representation of the bathymetric gradients ($\Delta h/h$), which is important for representing nonlinear interactions between currents and bathymetry. The modeled momentum balance was characterized by large spatial variability of the pressure gradient and horizontal advection terms over short distances, suggesting that observed inner-shelf momentum balances may be confounded. Given the available observational and modeling data, this work defines the spatially variable mean circulation and its formation mechanism—tidal rectification—and illustrates the importance of model resolution for resolving circulation and constituent exchange near the coast. The results of this study have implications for future observational and modeling studies near the MVCO and other inner-shelf locations with alongshore bathymetric variability.

Citation: Ganju, N. K., S. J. Lentz, A. R. Kirincich, and J. T. Farrar (2011), Complex mean circulation over the inner shelf south of Martha's Vineyard revealed by observations and a high-resolution model, *J. Geophys. Res.*, *116*, C10036, doi:10.1029/2011JC007035.

1. Introduction

[2] The mean circulation (i.e., low-frequency, quasi-steady circulation) over the inner shelf may be governed by tidal processes, baroclinic circulation, wind, waves, or some combination of these. Quantification and numerical modeling of the mean inner-shelf circulation is relevant to studies of heat budgets [*Wilkin*, 2006], water quality [*Rabalais et al.*, 1996], sediment transport [*Ferré et al.*, 2010], and larval transport [*Garland et al.*, 2002]. Limited observations, combined with assumptions of alongshore uniformity, are often interpreted to yield a comprehensive description of the circulation. Efforts to conduct spatially detailed observations are hampered by the large spatial scale of the inner shelf, the relatively large variations in bathymetry present in shallow inner-shelf waters, and the temporal scales at which forcings change. Recent efforts at cabled observatories or long-term mooring deployments address the issue of covering temporal variability on the inner shelf, though they are spatially limited.

[3] Locations with even subtle bathymetric features may confound interpretation of sparse in situ measurements and invalidate the assumption of alongshore-uniform flow. For example, mean flows can be generated by purely oscillatory tidal motions over variable bathymetry. *Robinson* [1981] elucidated the vorticity-generation mechanism that arises when tidal flows encounter bathymetric gradients; residual vorticity in these cases drives a tidally rectified flow. These flows are commonly associated with subtidal banks [*Loder*, 1980; *Chen and Beardsley*, 1995; *Chen et al.*, 1995] and headlands [*Signell and Geyer*, 1991]. *Chen and Beardsley* [1995] modeled tidally rectified flows over two-dimensional symmetric sand banks, generating along-isobath mean circulation that increased with bank slope and height in the unstratified case. *Signell and Geyer* [1991] described

[1]U.S. Geological Survey, Coastal and Marine Science Center, Woods Hole, Massachusetts, USA.
[2]Department of Physical Oceanography, Woods Hole Oceanographic Institution, Woods Hole, Massachusetts, USA.

0148-0227/11/2011JC007035

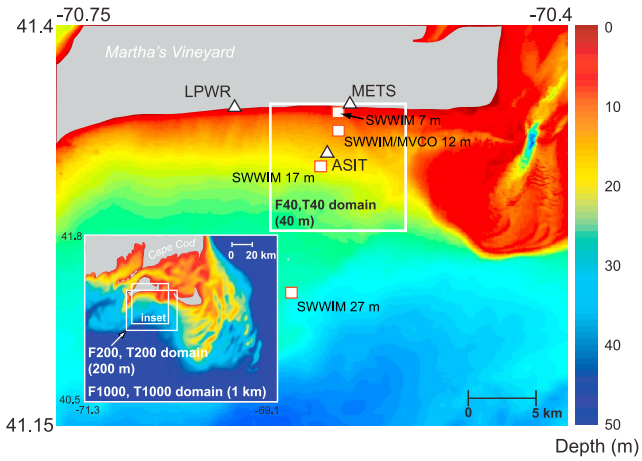

Figure 1. New England inner shelf, 1-km, and 200-m model grids (inset), and south shore of Martha's Vineyard with fixed ADCP (SWWIM), HF radar sites (LPWR, METS, ASIT), and 40-m model grid. U.S. East Coast grid not shown.

the headland-induced tidal rectification and mean circulation generated by oscillating currents. *Aretxabaleta et al.* [2008] modeled the gyre at the mouth of the Bay of Fundy, and by selectively adding and removing forcings, attributed its formation to tidal processes and density-driven circulation. These studies demonstrate that numerical modeling can separate tidal rectification from atmospheric and baroclinic forcing, but questions remain regarding the appropriate resolution needed to simulate tidal rectification in the inner-shelf environment.

[4] Model resolution is typically determined by a trade-off between computational power and the scales of interest. The coarsest possible resolution that represents the relevant processes is often selected, though this judgment is usually made by trial-and-error. For example, *Hurlburt and Hogan* [2000] found that while both coarse and fine simulations of the Atlantic were eddy-resolving, the coarsest domains did not generate strong eddies that could properly influence the mean flow. *Pohlmann* [2006], modeling coastal portions of the North Sea, suggested that a coarse domain could not resolve riverine freshwater flux, due to inaccurate representation of the coastline. The interaction of resolution and mean flows was studied by *Jones and Davies* [2007], who showed that finer resolution grids increased the detail of the mean flow field; the jaggedness of the coastline was also found to influence the solution significantly. In a comprehensive summary of resolution studies and issues, *Greenberg et al.* [2007] report on the importance of resolution for a number of oceanic and coastal studies, and also identify thresholds for possible error in open ocean and shelf-break situations. In the nearshore region, they stress the role of bathymetric gradient and coastline representation, but error thresholds are not presented.

[5] Nested modeling can potentially resolve coastal circulation features without excessive computational expense, by increasing model resolution as the domain of interest is approached. Nesting also obviates the need for high-resolution bathymetry over relatively large domains. *Penven et al.* [2006] presented a one-way nested model of the U.S. West Coast, and found that inner-grid solutions were greatly improved with the nesting procedure with only a slight increase in computational expense. *Barth et al.* [2008] demonstrated the efficacy of nesting a model of the West Florida Shelf instead of using climatological fields; shelf circulation was modified by the change in boundary conditions despite the open boundary being well offshore of the shelf.

[6] This study presents a comparison of recent observations and numerical modeling of the mean circulation over the inner shelf south of the island of Martha's Vineyard, along the eastern coast of the continental United States, during the late summer when wind and wave forcing are small. Surface currents from high-frequency radar and high-resolution nested modeling confirm the presence of a counter-clockwise gyre centered south of the Martha's Vineyard Coastal Observatory (MVCO). We build upon a prior model of the region [*He and Wilkin*, 2006] that represented large-scale barotropic forcing but did not have sufficient resolution to simulate circulation near the MVCO. We first present observational data, and then describe numerical experiments with three model domains with varying resolution and one-way nesting. Tide-only simulations are carried out to test the hypothesis that the mean circulation is largely driven by tidal processes, and constitutes a tidally rectified flow. We then describe the momentum balance of the mean alongshore flow, and the influence of the alongshore bathymetric slope. Finally, resolution issues and the importance of resolving bathymetric gradients are discussed.

2. Site Description and Observations

[7] Circulation south of the MVCO is influenced by regional patterns on the New England inner shelf (Figure 1). A predominantly westward, subtidal flow exists due to large scale pressure and buoyancy forcing, although seasonal variations in stratification and heat flux alter the structure of the flow field [*Shearman and Lentz*, 2003; *Fewings and Lentz*, 2010]. Tidal currents in the region are complex in this transition zone between the resonant response of the Gulf of Maine to the north and the Middle Atlantic Bight to the west [*Shearman and Lentz*, 2004; *He and Wilkin*, 2006].

[8] As part of the Stratification, Wind, and Waves on the Inner shelf of Martha's Vineyard (SWWIM) study, three broadband Acoustic Doppler Current Profilers (ADCPs) were deployed on bottom tripods over the inner shelf south of Martha's Vineyard from October 2006 through January 2010 (Figure 1). A 1200 kHz ADCP was deployed in 7-m water depth (0.4 km offshore) and two 600 kHz ADCPs in 17-m and 27-m water depth (3.8 km and 11.1 km offshore). The ADCPs typically recorded 5-min burst averages of 1 s samples every 20 min. Additionally, as part of the MVCO, a 1200 kHz ADCP has been deployed in 12-m water depth (1.6 km offshore) since August 2001, sampling continuously at 1 Hz. Monthly mean currents reveal a consistent annual cycle at all four SWWIM sites with small year-to-year variations in summer and larger year-to-year variations in winter due to stronger wind and wave forcing (Figures 2 and 3). Mean flows in September (the time period of overlapping coastal radar observations and model runs) are consistently westward, increasing from a few cm/s at the

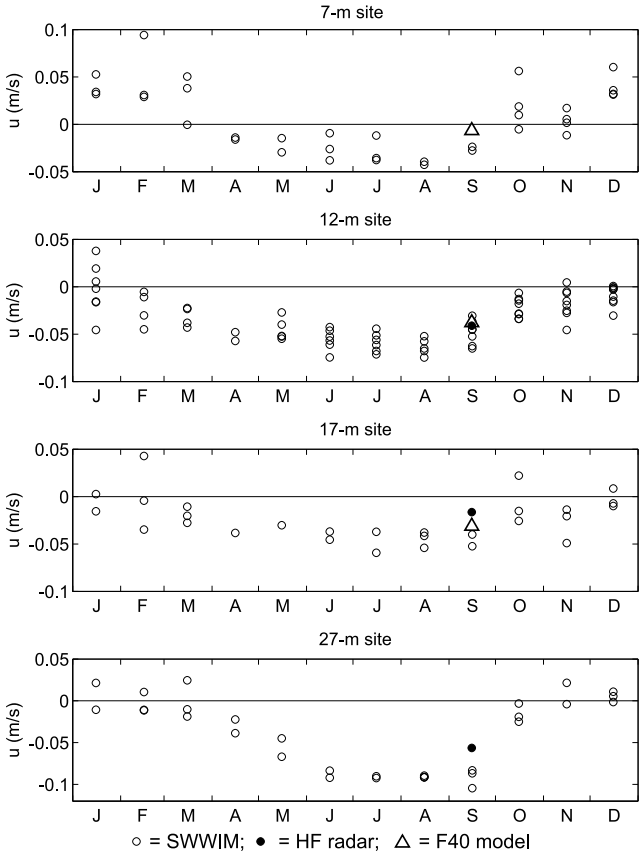

Figure 2. East/west (positive/negative) monthly mean depth-averaged velocities from SWWIM data (open circles), HF surface radar data (solid circle), and depth-averaged velocities from the full, unstratified 40-m model simulation (F40; triangle). SWWIM data span October 2006 to January 2010 with varying monthly coverage. HF surface radar data are from September 2010, and model results are from September 2007.

7-m site to ~10 cm/s at the 27-m site. Northward monthly means in August–September are near-zero at the 7-m and 12-m sites, 1–2 cm/s southward at the 17-m site and 1–2 cm/s northward at the 27-m site. The small year-to year variations in the monthly means for August and September provide justification for comparisons of mean flows from the model runs and coastal radar for different years.

[9] A high-frequency, CODAR-type coastal radar array was installed on the south shore of Martha's Vineyard in the summer of 2010 (Figure 1). The two land-based radar sites, located ~10 km apart with operating frequencies and bandwidths of 25 MHz and 350 kHz respectively, are able to observe surface currents at spatial resolutions approaching 400 m. Hourly averages of the combined, gridded surface current data collected from September 2010 are used for the present study. Comparisons between the near-surface ADCP-based velocities at the MVCO 12-m node (described above) and a time series of the co-located, radar-derived surface currents for this time period indicate that the initial setup of the radar system is able to observe the tidal currents at this location (~1.6 km offshore) with reasonable accuracies. RMS differences for the extracted M_2 tidal velocities observed by the radar and ADCP surface bins are 1.5 cm/s for both the east and north tidal components.

3. Numerical Modeling

3.1. Model Description

[10] We used the Community Sediment-Transport Modeling System (CSTMS) [*Warner et al.*, 2008], an open-source numerical modeling system that provides for two-way coupling of the Regional Ocean Modeling System (ROMS) with SWAN, an open-source wave model [*Booij et al.*, 1999]. ROMS is a three-dimensional, free surface, terrain-following numerical model that solves finite difference approximations of the Reynolds-averaged Navier-Stokes equations using the hydrostatic and Boussinesq assumptions [*Chassignet et al.*, 2000; *Haidvogel et al.*, 2000] with a split-explicit time stepping algorithm [*Shchepetkin and McWilliams*, 2005; *Haidvogel et al.*, 2008]. SWAN solves wave-averaged transport equations for wave action density (energy density divided by relative frequency) and accounts for shoaling, refraction, wind-wave generation, wave breaking, bottom dissipation, and nonlinear wave-wave interactions. Further details regarding the SWAN model are

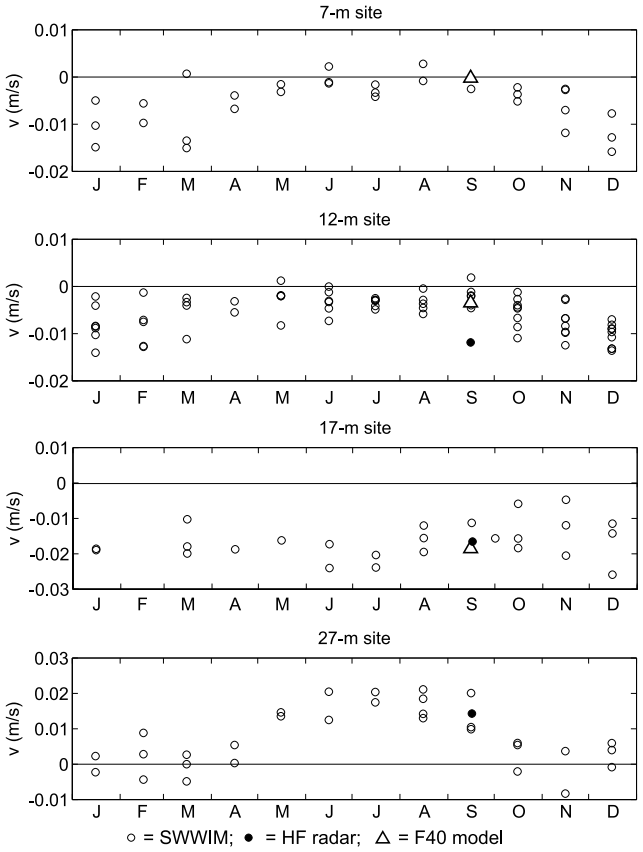

Figure 3. North/south (positive/negative) monthly mean depth-averaged velocities from SWWIM data (open circles), HF surface radar data (solid circle), and depth-averaged velocities from the full, unstratified 40-m model simulation (F40; triangle). SWWIM data span October 2006 to January 2010 with varying monthly coverage. HF surface radar data are from September 2010, and model results are from September 2007.

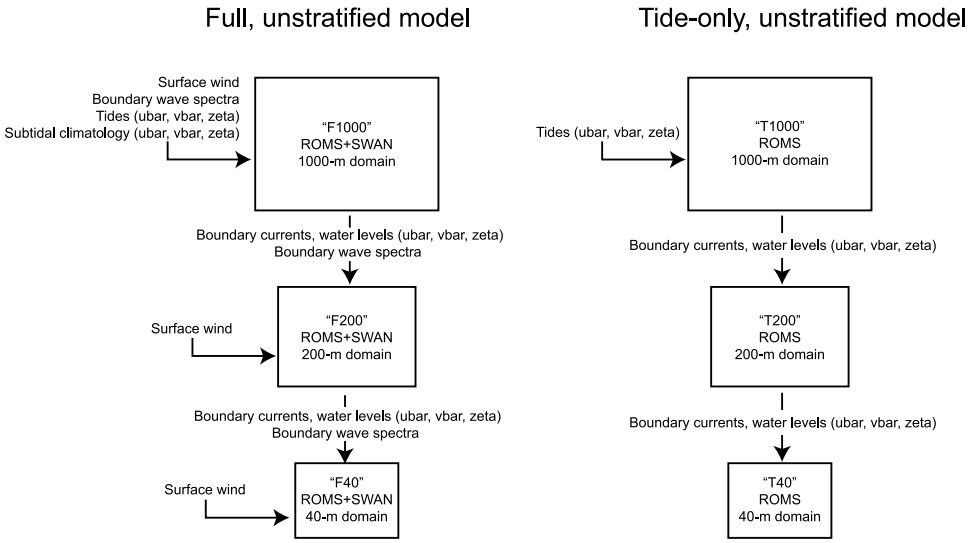

Figure 4. Schematic of model simulations, nesting hierarchy, and boundary forcing. Boundary wave spectra specify temporally and spatially varying frequency and directional wave energy; ubar and vbar refer to depth-averaged east–west and north–south currents, respectively; zeta refers to water levels.

documented by *Booij et al.* [1999]. Specific details for parameter specification, boundary conditions, and model coupling are included below.

3.2. Model Application

[11] The model runs performed here span the 23 August 2007 to 1 November 2007 period and are conducted on four grids of varying resolution in a fully three-dimensional mode (5 km; not shown, 1 km, 200 m, 40 m). The first set of simulations represents unstratified conditions with tidal, subtidal, wind, and wave forcing; the second set of simulations apply tidal forcing only (Figure 4). Using a series of idealized simulations, *Wilkin* [2006] demonstrated the dominance of tidal processes to the regional circulation, therefore ignoring baroclinic forcing is justified for these simulations. We used one-way grid nesting at all levels of resolution to provide boundary conditions for our numerical experiment. In one-way grid nesting applications, the coarser grid provides hydrodynamic information to the finer grid, but not vice versa. This can lead to discontinuities between computed solutions on the finer grid and boundary conditions from the coarser grid, but use of radiation conditions [*Flather*, 1976] allows the boundary conditions to relax in consideration of the computed solution. All simulations used depth-averaged velocity and water level for boundary forcing, with three-dimensional boundary velocity allowed to relax using a radiation condition.

3.2.1. Model Nesting and Coupling Methodology: "Full," Unstratified Case

[12] These simulations were conducted as detailed by *Ganju and Sherwood* [2010] and include atmospheric, subtidal (from a larger regional model), and wave forcing at all grid resolutions. We review only the fundamental details here. We ran the wave model SWAN on the coarsest grid (5-km resolution, "SWAN5km") for the entire U.S. East Coast, forcing with parametric time series of wave height, period, and direction from the Western North Atlantic model output of WAVEWATCH-III [*Tolman*, 1999], and wind components from the North American Mesoscale model [*Rogers et al.*, 2005]. In this case (at all grid resolutions), wave effects were restricted to increasing the apparent roughness in bottom boundary layer calculations following *Madsen* [1994], and were not considered for computation of radiation stresses or mass transport due to ongoing revision of the associated numerical methods.

[13] We then ran both ROMS and SWAN on an intermediate grid (F1000, Figure 4) with a domain encompassing southern New England at 1000-m resolution (Figure 1). At this resolution, the model was allowed to spin up for one week prior to 1 September 2007. Wave energy densities, as a function of frequency and direction through time, were extracted from the SWAN5km simulation and applied as boundary conditions at the edges for the F1000 simulation. Tidal forcing (water level and depth-averaged velocity) at the boundary was specified using K_1, O_1, Q_1, M_2, S_2, N_2, and K_2 tidal constituents following *Mukai et al.* [2002] while subtidal forcing (for water level and depth-averaged velocity) was provided by the MABGOM model (R. He, personal communication, 2008). In two-way coupled applications, ROMS passes fields of water level and velocity to SWAN, while SWAN passes wave height, wavelength, period, direction, and bottom orbital velocity. ROMS and SWAN were not coupled for the F1000 simulations, and test runs showed that two-way coupling generated only minor differences at significant computational expense.

[14] ROMS and SWAN were run using two-way coupling on a finer intermediate grid (F200, Figure 4) which represented the region south of Martha's Vineyard at 200-m resolution (Figure 1). Wave energy densities, as described above, were again extracted from the F1000 simulation and applied to the F200 grid for wave boundary conditions. Hydrodynamic boundary forcing was specified as time series of water level and depth-averaged velocity interpolated from the F1000 output. Two-way coupling between ROMS and SWAN was performed by passing computed fields at 10-min intervals. This procedure was repeated for

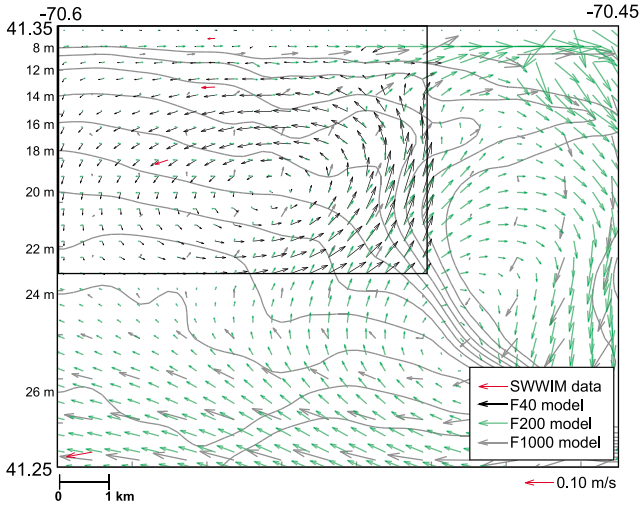

Figure 5. Comparison of depth-averaged velocity vectors between SWWIM and model output from the full, unstratified case at three resolutions. Inner box represents domain of 40-m grid.

the F40 simulation (Figure 4), with a 40-m horizontal resolution. Depth-averaged velocity components were averaged over the duration of each simulation (1 to 23 September 2007) to yield mean flow vectors.

3.2.2. Model Nesting and Coupling Methodology: Tidal, Unstratified Case

[15] We investigated tidal rectification processes by eliminating all forcings other than tidal harmonics using a similar nesting methodology (Figure 4). ROMS was run on the 1000-m domain with the aforementioned tidal forcing at the boundary (T1000). ROMS was subsequently run on a finer intermediate grid (T200) which represented the region south of Martha's Vineyard at 200-m resolution. Hydrodynamic boundary forcing was specified as time series of water level and depth-averaged velocity, interpolated from the T1000 output. Radiation conditions were specified for depth-averaged velocity following *Flather* [1976] and for water level following *Chapman* [1985]. This procedure was repeated for the T40 simulation with a 40-m horizontal resolution; boundary forcing was extracted from the T200 simulation. As above, depth-averaged velocity components were averaged over the duration of each simulation to yield mean flow vectors. This simulation eliminates surface momentum flux from winds, atmospheric heating and cooling, subtidal forcing from the MABGOM model, and wave-current interaction in the bottom boundary layer, which modulates the apparent roughness provided by the wave boundary layer, and therefore friction (the effect of the latter was investigated in detail by *Ganju and Sherwood* [2010]). Bottom friction is prescribed using a logarithmic drag formulation with a constant, uniform roughness height.

4. Results

4.1. Full, Unstratified Case

[16] Mean depth-averaged flows in the full, unstratified case varied with grid resolution (Figure 5). In the F1000 simulation, mean circulation was only in agreement with the offshore SWWIM station, where a westward jet is apparent in the surface currents from the HF radar as well (Table 1 and Figures 5 and 6). This barotropic jet was reproduced by *He and Wilkin* [2006] and attributed to the M_2 tidal residual. The jet begins east of the New England Shelf and includes residual circulation from the Gulf of Maine [*He and Wilkin*, 2006]. Recent studies suggest that this current is characterized by noticeably cooler waters [*Hong et al.*, 2009].

[17] In general, the F200 simulation follows the F1000 result; mean magnitudes are diminished despite similar tidal-timescale currents (Figure 5). At the MVCO location, alongshore tidal currents are similar between the F200 and F1000 simulations (±0.35 m/s). This suggests an interaction between radiation boundary conditions, bottom friction parameterization, and model resolution that modulates nonlinear interaction between the mean and tidal flow. The F200 simulation reproduces circulation at the offshore SWWIM station as well; a coherent cyclonic gyre near the MVCO does form at this resolution, though the magnitudes are reduced as compared to the F40 simulation.

[18] In the F40 simulation, a more pronounced counterclockwise gyre is developed in agreement with SWWIM and HF radar data (Figures 5 and 6). Inshore, the HF radar surface currents appear to diverge from the SWWIM depth-averaged means, perhaps due to differences in the surface versus depth-averaged currents. At all SWWIM sites the surface bin of the ADCPs are approximately 2 m below surface, hampering direct comparison with HF radar data. For the most part, near-surface SWWIM velocities are slightly larger than the depth-averaged means. Radar-based cross-shelf surface currents at these inshore locations between the radar stations have higher uncertainties due to geometric dilution of precision (i.e., loss of precision as the angle between stations and a given measurement location approach zero). Alongshore tidal currents in the F40 simulation are similar to the tidal currents from the F200 and F1000 simulations (±0.3 m/s). Taken independently, the SWWIM measurements confirm the northwestern side of

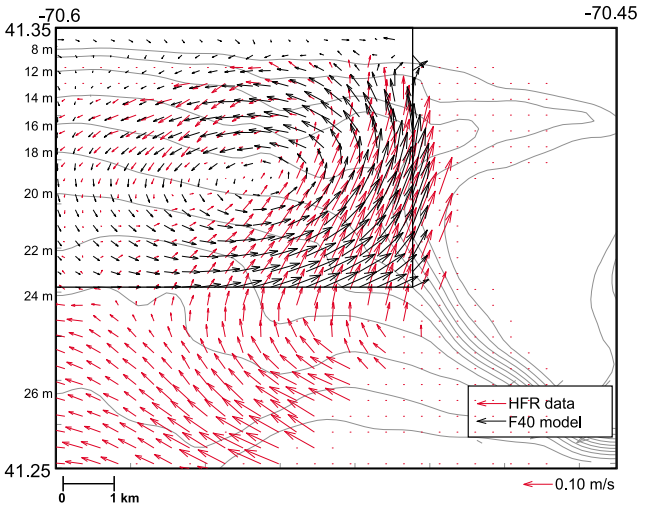

Figure 6. Comparison of surface velocity vectors between HF radar data and model output at finest resolution (F40 simulation). Inner box represents domain of 40-m grid.

Table 1. Comparison of SWWIM September Mean Flows With September 2007 Mean Model Results

	Observed		F1000		F200		F40	
Site	Speed (m/s)	Direction (deg)	Speed (m/s)	Direction (deg)	Speed (m/s)	Direction (deg)	Speed (m/s)	Direction (deg)
7 m	0.026	267	0.039	89	0.044	87	0.007	74
12 m	0.048	267	0.020	63	0.009	83	0.035	263
17 m	0.048	254	0.010	343	0.014	274	0.034	238
27 m	0.093	261	0.111	276	0.057	279	–	–

the gyre, and the HF data confirm the east side of the gyre. The deviation between the HF radar data and F40 result at the southern boundary may be due to bias in the model at the open boundary. In this portion of the domain, the F200 results appear to be in better agreement with the HF radar data. All three representations cover the same season over different years; therefore the similarity between them suggests that a common forcing mechanism is responsible. Due to the weak winds and waves during the late summer/early fall, tidal forcing was suspected as the dominant mechanism forcing the mean flow.

4.2. Tidal, Unstratified Case

[19] A tidally rectified mean circulation was evident from the tide-only simulations, with minor differences from the full, unstratified case. Similarly to that case, mean flows varied with grid resolution (Figure 7). Differences with the prior case arise due to wind and wave forcing, which affect surface momentum flux and bottom boundary layer calculations (for roughness), respectively. As with the full simulations, the T1000 simulation reproduced the westward offshore jet and not the inshore counter-clockwise gyre. However, the T200 simulation did partially reproduce the gyre with tidal forcing alone (albeit weaker than the T40 simulation). The fact that the gyre was present in the T200 simulation indicates that the bottom friction parameterization and tide-only boundary conditions slightly improved representation of the tidal rectification as compared to the F200 simulation. This is not surprising, and supports the hypothesis that tidal rectification is the dominant mechanism for the monthly mean circulation in September.

5. Discussion

5.1. Alongshore Momentum Balance of Tidally Rectified Flow

[20] We analyzed the diagnostic terms of the alongshore momentum balance from the T40 simulation model to interpret the underlying dynamics of the tidally rectified circulation. The depth-averaged terms in the alongshore momentum balance, ignoring wave effects, are

$$\frac{\partial u}{\partial t}+\left(u\frac{\partial u}{\partial x}+v\frac{\partial u}{\partial y}\right)-fv=-\frac{1}{\rho}\frac{\partial P}{\partial x}-\frac{\tau_x^b}{\rho h}+\upsilon\left(\frac{\partial^2 u}{\partial x^2}+\frac{\partial^2 u}{\partial y^2}\right) \quad (1)$$

where u is the depth-averaged alongshore x-direction velocity, v is the depth-averaged cross-shore y-direction velocity, f is the Coriolis parameter, P is the pressure, ρ is the water density, τ_x^b is the bottom stress, h is the water depth, and υ is the kinematic viscosity. These terms are as follows: first term is the local acceleration, second term is horizontal advection, third term is Coriolis force, fourth term is pressure gradient, fifth term is bottom stress, and the last term is horizontal viscosity.

[21] The tidally varying terms in the depth-averaged, alongshore (east-west) momentum balance from the tide-only, T40 simulation were extracted and averaged over a 25-h period. This 25-h mean did not vary significantly from the September mean; analogous terms in the cross-shore momentum balance were typically 50% smaller in comparison and therefore the alongshore terms are dominant. On the tidal timescale, the dominant terms (spatially averaged) were the pressure gradient, local acceleration, and horizontal advection; on the 25-h mean timescale (spatially averaged), the pressure gradient and horizontal advection became the dominant terms with a negligible contribution from local acceleration and greater influence of the Coriolis force; the sum of the pressure gradient, advection, and Coriolis force was balanced by bottom stress. *He and Wilkin* [2006], using the same 1000-m domain as this study, detailed the modeled momentum balances at three sites. At the deeper sites (h ~30 m), local acceleration was balanced by the Coriolis and pressure gradient terms. At the shallower site (h ~20 m) over Nantucket Shoals, the momentum balance was more congruent with the inner-shelf balance shown here, with pressure gradient balancing and advection.

[22] The spatial patterns of terms in the time-mean momentum balance are highly variable and correlated with subtle bathymetric changes (Figure 8). The modeled alongshore mean momentum balances indicate the dominance of the pressure gradient and horizontal advection terms, though the smaller Coriolis force has an important role in the spatial structure of the momentum balance

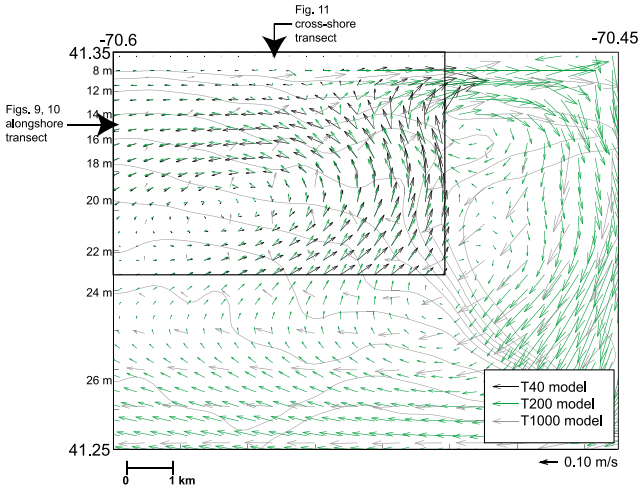

Figure 7. Mean depth-averaged circulation from tide-only simulations at three resolutions. Transect locations for Figures 9, 10, and 11 are shown.

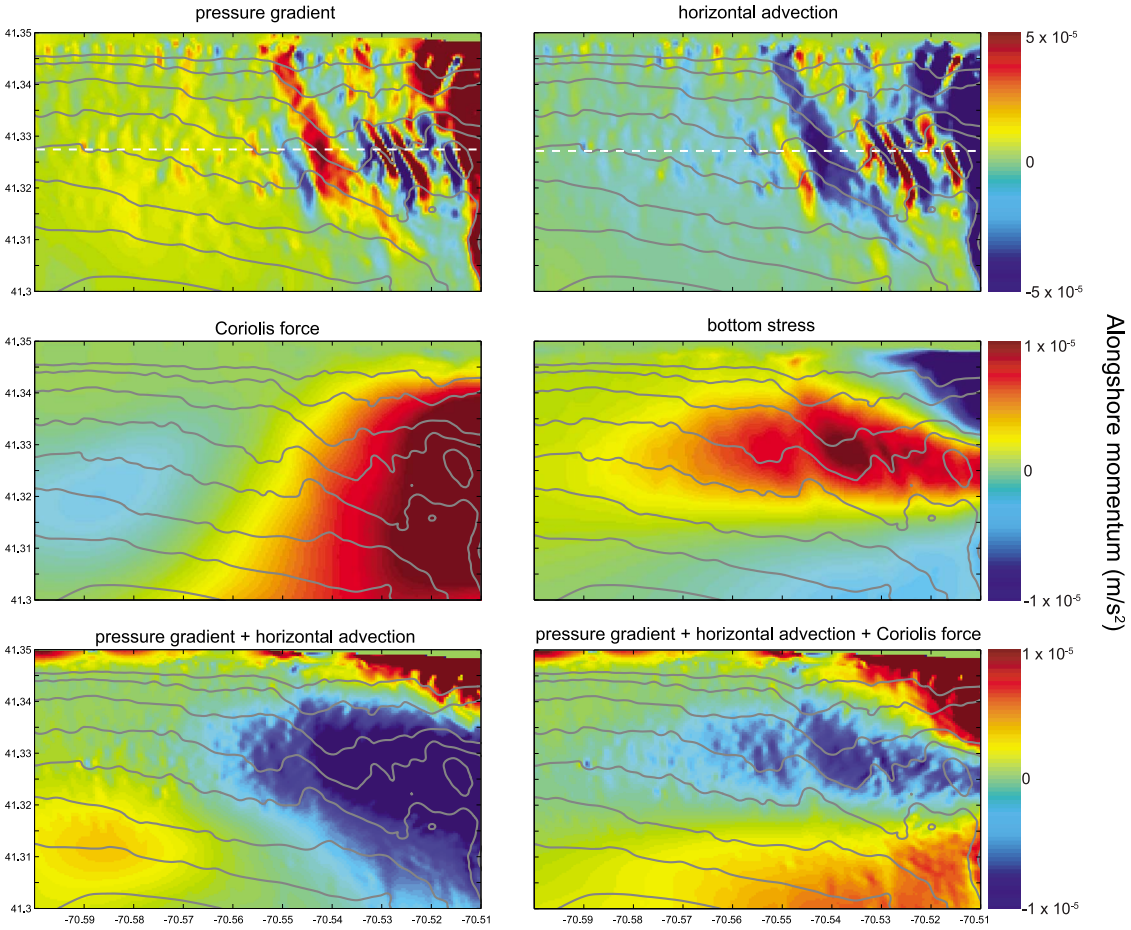

Figure 8. Spatial distribution of alongshore mean momentum terms for tide-only simulation (T40). Note scale change between top set of plots and middle/lower set. Isobaths begin at 8 m (top of image) and are spaced in 2 m intervals. White dotted line indicates transect used for Figures 9 and 10.

(Figure 8). The sum of these terms is largely balanced by the bottom stress. The spatial fluctuations of the pressure gradient and horizontal advection terms are correlated with the presence of the sorted bed forms, which are characterized by subtle bathymetric changes [*Goff et al.*, 2005]. We hypothesize that the tidal flow over these features gives rise to a Bernoulli-type effect: along a streamline, an increase in velocity is balanced by a decrease in pressure and vice versa. In this case the flow decelerates as the deeper portions of the sorted bed forms are encountered, and accelerates toward the shallower crests between the features resulting in a significant mean nonlinear acceleration term. The pressure gradient term varies in the alongshore direction in response to the alongshore bathymetric slope (dh/dx): the magnitude of the pressure gradient increases toward the troughs of the sorted bed forms, and decreases toward the crests (Figure 9). The horizontal advection term counters the pressure gradient, increasing toward bed form crests and decreasing toward the troughs. In the coarser T200 simulation the variation of these terms responds to the alongshore bathymetric slope, but with smaller oscillations congruent with the smaller alongshore bathymetric slope (due to larger resolution-dependent dx).

[23] We test the hypothesized interpretation of the dynamics outlined above by assuming a one-dimensional

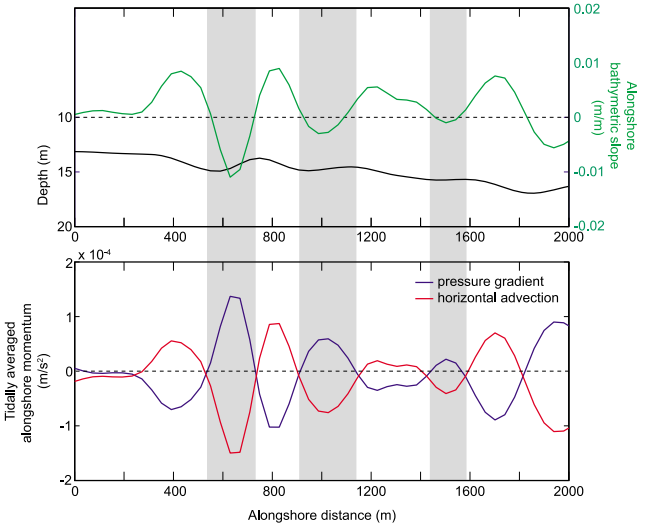

Figure 9. Alongshore depth and bathymetric slope, with corresponding terms from mean alongshore momentum balance of T40 simulation. The alongshore transect occupies the region of the strongest tidally rectified flow from the T40 simulation (Figure 7), shown with white dotted line in Figure 8. Gray bars are intended to highlight the correlation between the bathymetric slope and momentum terms.

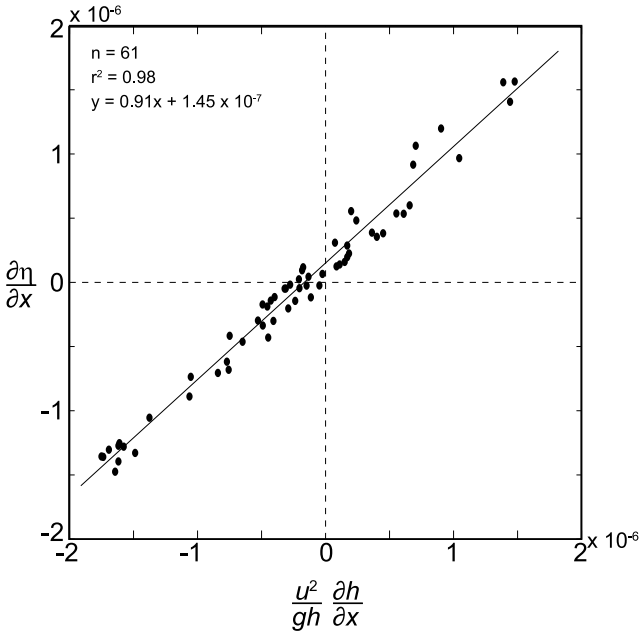

Figure 10. Linear fit between terms in equation (4), demonstrating a 1D alongshore balance between pressure gradient and horizontal advection. Data are extracted from an alongshore transect of the T40 simulation (Figure 7).

frame of reference for the alongshore flow; continuity implies that the longitudinal velocity gradient must be balanced by a longitudinal water level gradient, or

$$\frac{\partial u}{\partial x} \sim -\frac{u}{h}\frac{\partial h}{\partial x} \tag{2}$$

where u is the mean alongshore tidal velocity, x is the alongshore coordinate, and h is the water depth. As noted above and in Figure 9, horizontal advection and pressure gradient are largely in balance over the bathymetric features; again assuming this is primarily due to the alongshore component of flow:

$$u\frac{\partial u}{\partial x} \sim -g\frac{\partial \eta}{\partial x} \tag{3}$$

where η is the mean free-surface elevation. Substituting (2) in for the velocity gradient yields

$$\frac{\partial \eta}{\partial x} = \frac{u^2}{gh}\frac{\partial h}{\partial x} \tag{4}$$

Both sides of equation (4) were computed over a 25-h period from the T40 simulation using hourly data, near the 14-m isobath in the core of the alongshore jet (Figure 7). The alongshore tidal velocity u was computed as the mean of the absolute value of the tidal velocity over the 25-h period. The linear relationship with a slope close to unity supports the 1-D alongshore nature of the jet's momentum balance and its modulation by subtle bathymetric changes (Figure 10). The linear relationship and near-unity slope were also verified with hourly velocities and water levels (results not shown). The sensitivity of the momentum balance terms to relatively subtle bathymetric variability (0.01 m/m, or 0.4 m over a 40-m grid cell) points to a potential difficulty in using observational data from a few locations to compute mean momentum balances over any distance given the potential for large variations over short (unresolved) scales. However, this also suggests that it should be possible to estimate the short spatial scale component of the subtidal pressure gradient using only measurements of tidal velocity and high-resolution bathymetry. The high-resolution modeling of this region was instrumental in identifying the relationship between the pressure gradient and horizontal advection; below we assess how model resolution relates to accurate simulation of circulation.

5.2. Effect of Model Resolution on Mean Circulation

[24] These simulations demonstrate the impact of grid resolution on modeled mean circulation over the inner shelf. Several authors have demonstrated the effect of grid resolution on computed flows, and this study demonstrates a clear improvement in model performance (as compared with two independent data sets) as resolution is increased from 1000 m to 40 m. This provides an opportunity to assess how model resolution affects performance in this example. *Greenberg et al.* [2007] provide a useful framework to evaluate how resolution affects model solutions; here we briefly address some of the relevant topics from their review: open boundaries and nesting, coastline resolution, bathymetry, and vertical resolution.

[25] For all the simulations here, the boundary conditions for the finer domains are extracted from the coarser domain output, and imposed with radiation conditions that allow the boundary values to relax in relation to the solution computed within the domain. This accounts for discrepancies in mean flows at domain boundaries: the imposed velocity on the 200-m grid, taken directly from the 1000-m grid output, can be modulated based on the internal balance between the forcing and bottom friction. This suggests that there is interplay between boundary conditions and bottom friction that modifies mean circulation depending on grid resolution. It is likely that this dependence is related to the representation of bathymetry within the model domain, as realism increases with increased model resolution. The generation of vorticity due to bathymetric and topographic features is the likely cause for these discrepancies. Indeed, *Robinson*'s [1981] vorticity balance quantifies the dependence of vorticity generation mechanisms on bathymetric gradients in the alongshore and cross-shore directions. Further experimentation with idealized domains and multiple forcing cases (e.g., radiation versus clamped boundary conditions, variable adjustment timescales) may shed further light on the importance of boundary conditions for generating vorticity and mean circulation.

[26] *Greenberg et al.* [2007] examined the importance of the coastline in several idealized examples. In the system studied here, the relatively uniform coastline eliminates the common "staircase" effect tested in those examples. Instead, the inadequacy of the 1000-m model springs simply from the fact that the gyre's northern edge is only two grid cells from the land-sea boundary. This proximity, combined with the coarse representation of the nearshore bathymetry, prohibits a realistic representation of the tidal and mean flows. Similarly, the 200-m model contains 8 grid cells between the gyre and land; as the "grid-distance" is increased in the

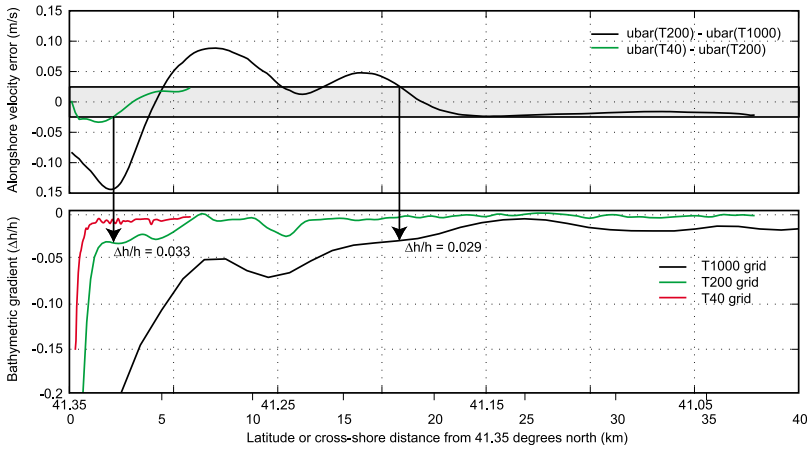

Figure 11. Divergence of coarse models from finer models (T1000 versus T200, T200 versus T40) in terms of alongshore depth-averaged velocity (ubar) in the cross-shore direction, and corresponding model cross-shore bathymetric gradient. Data are extracted from the cross-shore transect shown in Figure 7.

40-m model (to 40 cells) the representation of nearshore bathymetry obviously increases as well. Ultimately, the influence of the coastline cannot be separated from the influence of the nearshore bathymetric gradient in this case.

[27] *Loder* [1980] and *Greenberg et al.* [2007] identify the importance of the cross-shore bathymetric gradient, $\Delta h/h$, mainly in consideration of banks and shelf breaks respectively. The three domains used here represent a range of bathymetric gradients (over the same geographic area), and this likely affects the solution. Divergence in the solution for alongshore velocity (in the cross-shore direction) can be quantified by choosing an error threshold; we arbitrarily used a 10% deviation in the jet's tidal velocity (0.025 m/s). Comparing the T1000 and T200 results for alongshore velocity in the cross-shore direction (at a longitude of −70.56, in line with the MVCO) suggests that the T1000 model first exceeds the error threshold when $\Delta h/h$ exceeds about 0.03; the T200 model exceeds the error threshold at a similar value (Figure 11). *Greenberg et al.* [2007] cite higher acceptable values of $\Delta h/h$ (over 0.1); these results suggest that inner-shelf circulation requires finer representation of the bathymetric gradient than shelf-break or bank circulation studies (though our performance criteria are not identical). While the influence of the coastline may be partially responsible for the divergence in the model solutions within a few grid cells from shore, the coarser models diverge more than 15 cells from shore in both the T1000 and T200 models, and the coastline is not expected to affect the solution at this distance.

5.3. Capturing Spatial Variability of Inner-Shelf Circulation

[28] The observational data and model simulations demonstrate the difficulty in characterizing the mean circulation on the inner shelf. Using this case as an example, the long-term SWWIM data from four cross-shore moorings are too sparse to characterize the cross-shore spatial structure of the mean depth-averaged circulation and they provide no information about the alongshore structure of the flow. However, the data do provide a suitable data set for model confirmation. In fact, the data are essential to identifying the required model resolution: only the F40 model reproduces SWWIM data at the inshore stations. The spatial pattern revealed by the F40 model is then bolstered by the surface radar data, which provides a detailed picture of the spatial structure of the near-surface flow and validates the eastern half of the simulated gyre, though discrepancies at the southern edge of the gyre remain. These three approaches – fixed ADCP deployments, surface radar arrays, and high-resolution numerical modeling – each serve distinct functions that support the other methods. Observational programs that aim to capture inner-shelf circulation could conceivably deploy these approaches in specific order to minimize instrumentation needs and maximize the utility of collected data. Preliminary modeling of the region, with high-resolution, nested grids, would indicate the importance of bathymetric features and the possible complexity of mean circulation. ADCP deployments can then be situated across transects with the greatest variability: in this case, a cross-shore deployment through the center of the gyre would capture the strongest areas of mean circulation. Finally, surface radar can be employed to resolve spatial patterns of the near-surface velocity and the relationship with the modeled surface velocity.

6. Summary and Conclusions

[29] This study presents a comparison of recent observational and modeling efforts in an overlapping domain near the Martha's Vineyard Coastal Observatory. The combined results define the spatially variable September–mean circulation, and identify its driver to be tidal rectification. The modeling results also demonstrate the effect of model resolution on resolving circulation features near the coast. The September–mean circulation south of Martha's Vineyard, Massachusetts, was measured using long-term fixed ADCP measurements, a newly installed high-frequency radar system measuring surface currents, and modeled using the Regional Ocean Modeling System with a series of nested grids at 1000-m, 200-m, and 40-m resolutions. The three independent methods, although applied for different years,

verified a complex September–mean circulation that is dominated by a counter-clockwise gyre centered south of the Martha's Vineyard Coastal Observatory. Further model runs, with all forcings other than tides removed, retained this circulation feature, pointing to tidal rectification as the mechanism responsible for the mean circulation pattern. At the 40-m grid resolution, the mean momentum balances are dominated by the pressure gradient and horizontal advection terms, which vary coherently with subtle bathymetric changes over sorted bed forms. Further analysis shows that in the core of the alongshore velocity jet (northern half of the gyre), the flow is essentially an alongshore Bernoulli-type balance, and thus the small-scale pressure gradient can be calculated using the tidal velocity and bathymetry data alone. Comparing the coarse model results with finer model results suggests that model solutions diverge from each other at modeled cross-shore bathymetric gradients ($\Delta h/h$) of about 0.03, considerably less than prior work over sandbanks and shelf breaks suggests. Both the observations and modeling point to the inherent difficulty of observing and modeling inner-shelf circulation over long timescales, and calculating momentum balances in areas with subtle bathymetric features. Future studies of inner-shelf circulation should employ combined observational and modeling techniques to optimally capture spatial and temporal variability over seemingly straightforward domains.

[30] **Acknowledgments.** Funding was provided through the Office of Naval Research Ripples DRI, U.S. Geological Survey Coastal and Marine Geology Program, and National Science Foundation. Use of firm names is for descriptive purposes only and does not imply endorsement by the U.S. Government. Input from Chris Sherwood, Marlene Noble, Rich Signell, John Warner, and the three anonymous reviewers greatly improved the study. Ruoying He provided the U.S. East Coast grid used in this study.

References

Aretxabaleta, A. L., D. J. McGillicuddy, K. W. Smith, and D. R. Lynch (2008), Model simulations of the Bay of Fundy Gyre: 1. Climatological results, *J. Geophys. Res.*, *113*, C10027, doi:10.1029/2007JC004480.

Barth, A., A. Alvera-Azcárate, and R. H. Weisberg (2008), Benefit of nesting a regional model into a large-scale ocean model instead of climatology. Application to the West Florida Shelf, *Cont. Shelf Res.*, *28*, 561–573.

Booij, N., R. C. Ris, and L. H. Holthuijsen (1999), A third-generation wave model for coastal regions: 1. Model description and validation, *J. Geophys. Res.*, *104*(C4), 7649–7666, doi:10.1029/98JC02622.

Chapman, D. C. (1985), Numerical treatment of cross-shelf open boundaries in a barotropic coastal ocean model, *J. Phys. Oceanogr.*, *15*, 1060–1075, doi:10.1175/1520-0485(1985)015<1060:NTOCSO>2.0.CO;2.

Chassignet, E. P., H. Arango, D. Dietrich, T. Ezer, M. Ghil, D. B. Haidvogel, C. C. Ma, A. Mehra, A. M. Paiva, and Z. Sirkes (2000), DAMÉE-NAB: The base experiments, *Dyn. Atmos. Oceans*, *32*(3–4), 155–183, doi:10.1016/S0377-0265(00)00046-4.

Chen, C., and R. C. Beardsley (1995), A numerical study of stratified tidal rectification over finite-amplitude banks. Part I: Symmetric banks, *J. Phys. Oceanogr.*, *25*, 2090–2110, doi:10.1175/1520-0485(1995)025<2090:ANSOST>2.0.CO;2.

Chen, C., R. C. Beardsley, and R. Limeburner (1995), A numerical study of stratified tidal rectification over finite-amplitude banks. Part II: Georges Bank, *J. Phys. Oceanogr.*, *25*, 2111–2128, doi:10.1175/1520-0485(1995)025<2111:ANSOST>2.0.CO;2.

Ferré, B., C. R. Sherwood, and P. L. Wiberg (2010), Sediment transport on the Palos Verdes shelf, California, *Cont. Shelf Res.*, *30*, 761–780, doi:10.1016/j.csr.2010.01.011.

Fewings, M. R., and S. J. Lentz (2010), Momentum balances on the inner continental shelf at Martha's Vineyard Coastal Observatory, *J. Geophys. Res.*, *115*, C12023, doi:10.1029/2009JC005578.

Flather, R. A. (1976), A tidal model of the northwest European continental shelf, *Mem. Soc. R. Sci. Liege*, *6*, 141–164.

Ganju, N. K., and C. R. Sherwood (2010), Effect of roughness formulation on the performance of a coupled wave, hydrodynamic, and sediment transport model, *Ocean Modell.*, *33*, 299–313, doi:10.1016/j.ocemod.2010.03.003.

Garland, E. D., C. A. Zimmer, and S. J. Lentz (2002), Larval distributions in inner-shelf waters: The roles of wind-driven cross-shelf currents and diel vertical migrations, *Limnol. Oceanogr.*, *47*, 803–817, doi:10.4319/lo.2002.47.3.0803.

Goff, J. A., L. A. Mayer, P. Traykovski, I. Buynevich, R. Wilkens, R. Raymond, G. Glang, R. L. Evans, H. Olson, and C. Jenkins (2005), Detailed investigation of sorted bedforms, or "rippled scour depressions," within the Martha's Vineyard Coastal Observatory, Massachusetts, *Cont. Shelf Res.*, *25*(4), 461–484, doi:10.1016/j.csr.2004.09.019.

Greenberg, D. A., F. Dupont, F. H. Lyard, D. R. Lynch, and F. E. Werner (2007), Resolution issues in numerical models of oceanic and coastal circulation, *Cont. Shelf Res.*, *27*, 1317–1343, doi:10.1016/j.csr.2007.01.023.

Haidvogel, D. B., H. G. Arango, K. Hedstrom, A. Beckmann, P. Malanotte-Rizzoli, and A. F. Shchepetkin (2000), Model evaluation experiments in the North Atlantic Basin: Simulations in nonlinear terrain-following coordinates, *Dyn. Atmos. Oceans*, *32*(3–4), 239–281, doi:10.1016/S0377-0265(00)00049-X.

Haidvogel, D. B., et al. (2008), Ocean forecasting in terrain-following coordinates: Formulation and skill assessment of the Regional Ocean Modeling System, *J. Comput. Phys.*, *227*(7), 3595–3624, doi:10.1016/j.jcp.2007.06.016.

He, R., and J. L. Wilkin (2006), Barotropic tides on the southeast New England shelf: A view from a hybrid data assimilative modeling approach, *J. Geophys. Res.*, *111*, C08002, doi:10.1029/2005JC003254.

Hong, X., P. J. Martin, S. Wang, and C. Rowley (2009), High SST variability south of Martha's Vineyard: Observation and modeling study, *J. Mar. Syst.*, *78*, 59–76, doi:10.1016/j.jmarsys.2009.03.001.

Hurlburt, H. E., and P. J. Hogan (2000), Impact of 1/8° to 1/64° resolution on Gulf Stream model-data comparisons in basin-scale subtropical Atlantic Ocean models, *Dyn. Atmos. Oceans*, *32*, 283–329, doi:10.1016/S0377-0265(00)00050-6.

Jones, J. E., and A. M. Davies (2007), On the sensitivity of tidal residuals off the west coast of Britain to mesh resolution, *Cont. Shelf Res.*, *27*, 64–81, doi:10.1016/j.csr.2006.09.003.

Loder, J. W. (1980), Topographic rectification of tidal currents on the sides of Georges Bank, *J. Phys. Oceanogr.*, *10*, 1399–1416, doi:10.1175/1520-0485(1980)010<1399:TROTCO>2.0.CO;2.

Madsen, O. S. (1994), Spectral wave-current bottom boundary layer flows, paper presented at 24th International Conference, Coastal Eng. Res. Counc., Kobe, Japan.

Mukai, A., J. Westerink, R. Luettich, and D. Mark (2002), Eastcoast 2001: A tidal constituent database for the western North Atlantic, Gulf of Mexico and Caribbean Sea, *Tech. Rep. ERDC/CHL TR-02-24*, Coastal and Hydraul. Lab., U.S. Army Eng. Res. and Dev. Cent., Vicksburg, Miss.

Penven, P., L. Debreu, P. Marchesiello, and J. C. McWilliams (2006), Evaluation and application of the ROMS 1-way embedding procedure to the central California upwelling system, *Ocean Modell.*, *12*, 157–187, doi:10.1016/j.ocemod.2005.05.002.

Pohlmann, T. (2006), A meso-scale model of the central and southern North Sea: Consequences of an improved resolution, *Cont. Shelf Res.*, *26*, 2367–2385, doi:10.1016/j.csr.2006.06.011.

Rabalais, N., R. Turner, D. Justic, Q. Dortch, W. Wiseman, and B. Sen Gupta (1996), Nutrient changes in the Mississippi River and system responses on the adjacent continental shelf, *Estuaries Coasts*, *19*, 386–407, doi:10.2307/1352458.

Robinson, I. S. (1981), Tidal vorticity and residual circulation, *Deep Sea Res., Part A*, *28*, 195–212, doi:10.1016/0198-0149(81)90062-5.

Rogers, E., Y. Lin, K. Mitchell, W.-S. Wu, B. Ferrier, G. Gayno, M. Pondeca, M. Pyle, V. Wong, and M. Ek (2005), The NCEP North American mesoscale modeling system: Final Eta model/analysis changes and preliminary experiments using the WRF-NMM, in *Proceedings of the 21st Conference on Weather Analysis and Forecasting/17th Conference on Numerical Weather Prediction*, p. 4B.5, Am. Meteorol. Soc., Boston, Mass.

Shchepetkin, A. F., and J. C. McWilliams (2005), The regional oceanic modeling system (ROMS): A split-explicit, free-surface, topography-following-coordinate oceanic model, *Ocean Modell.*, *9*(4), 347–404, doi:10.1016/j.ocemod.2004.08.002.

Shearman, R. K., and S. J. Lentz (2003), Dynamics of mean and subtidal flow on the New England shelf, *J. Geophys. Res.*, *108*(C8), 3281, doi:10.1029/2002JC001417.

Shearman, R. K., and S. J. Lentz (2004), Observations of tidal variability on the New England shelf, *J. Geophys. Res.*, *109*, C06010, doi:10.1029/2003JC001972.

Signell, R. P., and W. R. Geyer (1991), Transient eddy formation around headlands, *J. Geophys. Res.*, *96*(C2), 2561–2575, doi:10.1029/90JC02029.

Tolman, H. L. (1999), User manual and system documentation of WAVEWATCH-III version 1.18, *NOAA/NWS OMB Contrib. 166*, 110 pp., Natl. Weather Serv., Camp Springs, Md.

Warner, J. C., C. R. Sherwood, R. P. Signell, C. K. Harris, and H. G. Arango (2008), Development of a three-dimensional, regional, coupled wave, current, and sediment-transport model, *Comput. Geosci.*, *34*(10), 1284–1306, doi:10.1016/j.cageo.2008.02.012.

Wilkin, J. L. (2006), The summertime heat budget and circulation of southeast New England shelf waters, *J. Phys. Oceanogr.*, *36*, 1997–2011, doi:10.1175/JPO2968.1.

N. K. Ganju, U.S. Geological Survey, Coastal and Marine Science Center, 384 Woods Hole Rd., Woods Hole, MA 02543, USA. (nganju@usgs.gov)

J. T. Farrar, A. R. Kirincich, and S. J. Lentz, Department of Physical Oceanography, Woods Hole Oceanographic Institution, 384 Woods Hole Rd., Woods Hole, MA 02543, USA.